Journal of Physics: Conference Series **651** (2015) 012018 doi:10.1088/1742-6596/651/1/012018

QCD Phase Diagram and the Constant Mass Approximation

A. Ahmad[1,2], A. Ayala[3], A. Bashir[1], E. Gutiérrez[1], A. Raya[1,4].

[1]Instituto de Física y Matemáticas, Universidad Michoacana de San Nicolás de Hidalgo. Edificio C-3, Ciudad Universitaria, Morelia 58040, Michoacán, México.
[2]Department of Physics, Gomal University, 29220, D.I. Khan, K.P.K., Pakistan.
[3]Instituto de Ciencias Nucleares, Universidad Nacional Autónoma de México. Circuito Exterior s/n. Apartado Postal 70-543, C.P. 04510, México, D.F., México.
[4] Facultad De Ciencias, Pontificia Universidad Católica de Chile, Casilla 306, Santiago 22, Chile.

E-mail: (aftabahmad@ifm.umich.mx, ayala@nucleares.unam.mx, adnan@ifm.umich.mx, enif@ifm.umich.mx, raya@ifm.umich.mx)

Abstract. Dynamical generation of quark masses in the infrared region of QCD plays an important role to understand the peculiar nature of the physics of hadrons. As it is known, the solution of QCD gap equation for the quark mass function is flat for low momentum, but smoothly evolves to the perturbative behavior at high momentum. In this work, we use an effective truncation of QCD gap equation valid up to 1 GeV, and implement it at finite temperature and chemical potential to understand the QCD phase diagram for chiral symmetry breaking-chiral symmetry restoration, and confinement-deconfinement phase transitions from the Schwinger-Dysin equations point of view. Our effective kernel contains a gluon dressing function with two light quark flavors $N_f = 2$, with current quark mass 0.0035 GeV. An effective coupling, adjusted to reproduce the behavior of the chiral condensate at finite T complements our truncation. We find the critical end point of the phase diagram located at the temperature $T^E = 0.1245$ GeV and the baryonic chemical potential $\mu_B^E = 0.211$ GeV.

1. Introduction

QCD at finite temperature and chemical potential plays an important role to understand the different transitions that took place in the early universe, after a few micro seconds from the Big Bang. As it is known, the observable degrees of freedom of quantum chromodynamics (QCD) at low temperature are the color-singlet hadrons, while at high temperature, the interaction between quark and gluons becomes weaker, causing hadrons to split up in a new phase where the dominant degrees of freedom are the quarks and gluons. This type of phase transition is referred to as confinement-deconfinement transition.

The vanishing of dynamically generated quark mass at high temperature T and/or chemical potential μ corresponds to another type of transition i.e., chiral symmetry restoration, while at zero T and μ, chiral symmetry is broken. Thus, when the strength of the QCD interaction diminishes with increasing T and μ, only the current quark masses survive when T and μ exceed a set of critical values. This is the chiral symmetry breaking-restoration phase transition. As for experiment is concerned, implications of chiral symmetry breaking for the elastic and transition form factors of mesons and baryons form an integral part of the planned program at the 12

GeV upgrade of the Thomas Jefferson National Accelerator Facility in Virginia [1]. There are other experiments around the world that might help to understand the confinement and chiral transitions like RHIC in Brookhaven, LHC at CERN, and future experiment proposals like CBM at FAIR, in Germany.

In this work we use the Schwinger-Dyson Equations (SDE) approach to study the above mentioned phase transitions from first principles. We exploit the idea that dynamically generated masses for the quark are constants in the infrared region for momentum lower than 1 GeV, and promote this to finite temperature and density to understand the QCD phase transitions. For our effective kernel, we use a model for the gluon propagator which is consistent with the refined Gribov-Zwanziger scenario for confinement and is in agreement with lattice QCD. We consider the case in which the propagator has quark flavor dependence, Ref. [2], and dress our kernel with a momentum dependent effective coupling as in Refs. [3, 4]. We calculate the chiral quark condensate for different values of temperature and match with lattice data, Ref. [5], at finite temperature. We then extend this parametriazation of the condensate at finite density. For the confinement-deconfinement transition, we use the spatial average of the scalar part of the quark propagator at zero spatial and explore violation of reflection positivity. The contribution is organized as follows: In. Sect. 2 we present the SDE for the quark propagator at finite temperature and density. Section 3 is devoted to introduce the Constant Mass Approximation and our effective kernel. Discussion and conclusions of our findings are presented in Sect. 4.

2. QCD Gap Equation at $T \neq 0$ and $\mu \neq 0$

The quark propagator is a basic object to analyze dynamical chiral symmetry breaking and confinement. At finite T and μ, we start from the general form of this two-point function

$$S^{-1}(\vec{p},\widetilde{\omega}_n) = (i\vec{\gamma}.\vec{p})A(\vec{p}^2,\widetilde{\omega}_n^2) + i\gamma_0\widetilde{\omega}_n C(\vec{p}^2,\widetilde{\omega}_n^2) + B(\vec{p}^2,\widetilde{\omega}_n^2), \tag{1}$$

where $\widetilde{w}_n = w_n + i\mu$, with μ representing the chemical potential and $w_n = (2n+1)\pi T$ are the fermionic Matsubara frequencies. $A(\vec{p}^2,\tilde{w}_n^2)$, $B(\vec{p}^2,\tilde{w}_n^2)$ and $C(\vec{p}^2,\tilde{w}_n^2)$ are the scalar functions to be self consistently determined through solving the corresponding SDE or gap equation

$$S^{-1}(\vec{p},\widetilde{\omega}_n) = (i\vec{\gamma}\cdot\vec{p}) + i\gamma_0\widetilde{\omega}_n + m + \Sigma(\vec{p},\widetilde{\omega}_n), \tag{2}$$

in which m is the bare mass for the quark, the self energy has the form

$$\Sigma(\vec{p},\widetilde{\omega}_n) \;=\; T\sum_{l=-\infty}^{l=+\infty}\int\frac{d^3\vec{k}}{(2\pi)^3}g^2 D_{\mu\nu}(\vec{p}-\vec{k},\Omega_{nl};T,\mu)\frac{\lambda^a}{2}\gamma_\mu S(\vec{k},\omega_l)\frac{\lambda^a}{2}\Gamma_\nu(\vec{k},\vec{p},\tilde{\omega}_l,\tilde{\omega}_n), \tag{3}$$

$\Omega_{nl} = \omega_n - \omega_l$ and $\Gamma_\nu(\vec{k},\vec{p},\tilde{\omega}_l,\tilde{\omega}_n)$ is the full quark-gluon vertex. Due to the heat bath, the gluon propagator splits into longitudinal and transverse parts, namely

$$D_{\mu\nu}(\vec{q}^2,\Omega_{nl}^2) = P^T_{\mu\nu}D^T(\vec{q}^2,\Omega_{nl}^2) + P^L_{\mu\nu}D^L(\vec{q}^2,\Omega_{nl}^2,m_D^2). \tag{4}$$

The longitudinal part is modified by an extra term, the Debye screening mass $m_D^2 = (4/3)T^2 + \mu^2/\pi^2$ [6]. In Eq. (4), $P^T_{\mu\nu}$ is the transverse and $P^L_{\mu\nu}$ is the longitudinal projection operators, given by $P^L_{\mu\nu} = \delta_{\mu\nu} - Q_\mu Q_\nu/Q^2 - P^T_{\mu\nu}$, $P^T_{44} = P^T_{00} = 0$, $P^T_{ij} = \delta_{ij} - q_i q_j/\vec{q}^2$. We complete our gap equation kernel by considering

$$g^2 D_{\mu\nu}(\vec{q}^2,\Omega_{nl}^2)\Gamma_\nu(\vec{k},\vec{p},\omega_l,\omega_n) \to g^2_{eff}(\vec{q}^2,\Omega_{nl}^2)D_{\mu\nu}(\vec{q}^2,\Omega_{nl}^2)\zeta(T)\gamma_\nu, \tag{5}$$

where we introduce $\zeta(T)$ to match with the lattice results.

3. Constant Mass Approximation

The constant mass approximation approach (CMA) has been motivated in the field of magnetic catalysis of dynamical chiral symmetry breaking [7]. It is based on the observation that the kernel of gap equation yields only contribution from the small momentum region, where the mass function is roughly constant. From Eqs.(1) and (2), and using our effective kernel, Eq. (5), after taking the trace we reach to the following expression for our $B(\vec{p}^2,\tilde{w}_n^2)$ function

$$\begin{aligned} B(\vec{p}^2,\tilde{\omega}_n^2) &= m \\ &-\frac{4}{3}T\zeta(T)\sum_{l=-\infty}^{l=+\infty}\int\frac{d^3\vec{k}}{(2\pi)^3}\sigma_B(\vec{k}^2,\tilde{\omega}_l^2)g_{eff}^2(\vec{q}^2,\Omega_{nl}^2)\Big[D^L(\vec{q}^2,\Omega_{nl}^2,m_D^2)+2D^T(\vec{q}^2,\Omega_{nl}^2)\Big]. \end{aligned} \quad (6)$$

Here $\sigma_B(\vec{p}^2,\tilde{\omega}_n^2) = -B(\vec{p}^2,\tilde{\omega}_n^2)/(\vec{p}^2A^2(\vec{p}^2,\tilde{\omega}_n^2)+\tilde{\omega}_n^2C^2(\vec{p}^2,\tilde{\omega}_n^2)+B^2(\vec{p}^2,\tilde{\omega}_n^2))$. The mass function for the quark is $M(\vec{p}^2,\tilde{\omega}_n^2) = B(\vec{p}^2,\tilde{\omega}_n^2)/A(\vec{p}^2,\tilde{\omega}_n^2)$. We set $A(\vec{k}^2,\tilde{\omega}_l^2) = C(\vec{k}^2,\tilde{\omega}_l^2) = 1$. We further take $\vec{p}=0$ and take all the B functions to be independent of momentum. Replacing $B(\vec{p}^2=0,\tilde{w}_n^2) = M_0(\tilde{w}_n^2)$, we have the following tower of relations of constant masses for every Matsubara frequency

$$\begin{aligned} M_0(\tilde{\omega}_n^2) &= m \\ &+\frac{2T\zeta(T)}{\pi^2}\sum_l\int_0^{\Lambda^2}dk\vec{k}^2\frac{M_0(\tilde{\omega}_l^2)g_{eff}^2(\vec{k}^2,\Omega_{nl}^2)}{\vec{k}^2+\tilde{\omega}_l^2+M_0^2(\tilde{\omega}_l^2)}\Big[D^L(\vec{k}^2,\Omega_{nl}^2,m_D^2)+2D^T(\vec{k}^2,\Omega_{nl}^2)\Big]. \end{aligned} \quad (7)$$

For the gluon propagator, we take $D^L(K,m_D^2) = D^T(K,0)\equiv D(K)$, where we have selected the following form of the flavor dependent dressing for the gluon in Landau gauge

$$D(K^2) = \frac{K^2+M_1^2}{K^4+K^2(M_1^2-\frac{13g_1^2<A_1^2>}{24})+M_1^2m_0^2}, \quad (8)$$

where $K^2=\vec{k}^2+\Omega_{nl}^2$. The parameters in this dressing function are the following: $M_1=4.85$ [GeV^2], which is related to the condensate of auxiliary fields emerging when incorporating the horizon condition to the action, $g_1^2 < A_1^2 >= 0.474(16.406-N_f)$ [GeV^2] is related to the dimension-two gluon condensate and $m_0 = 1.011(9.161-N_f)^{-1/2}$ [GeV^2]. We complete our kernel with the effective interaction $g_{eff}^2(\vec{k}^2,\Omega_{nl}^2) = 4\pi a_2\nu(\vec{k}^2,\Omega_{nl}^2)$ where $\nu(\vec{k}^2,\Omega_{nl}^2)$ is given by as in Refs. [3, 4] by

$$\nu(K^2) = \left[\frac{a+b\left(\frac{K}{\Lambda}\right)^2}{1+c\left(\frac{K}{\Lambda}\right)^2+d\left(\frac{K}{\Lambda}\right)^4+o\left(\frac{K}{\Lambda}\right)^6+\frac{\pi\gamma}{\log\left[e+\left(\frac{K}{\Lambda}\right)^2\right]}}\right], \quad (9)$$

with $a=1.47$; $b=0.881$; $c=0.314$; $d=0.00986$; $o=0.00168$; $\gamma=12/25$; $\Lambda=0.234$; $a_2=0.7$. The parameter $\zeta(T)$ is fitted with lattice data is in the form (see discussion below)

$$\zeta(T) = \frac{a_1+b_1T+c_1T^2}{1+d_1T+e_1T^2+f_1T^3} \quad (10)$$

where $a_1=0.355$; $b_1=-2.83$; $c_1=6.627$; $d_1=-6.74$; $e_1=4.45$; $f_1=43.35$. The chiral condensate, in our case is

$$-<\bar{\psi}\psi>=\frac{2N_cT}{\pi^2}\sum_n\int_0^{\Lambda^2}dk\vec{k}^2\frac{M_0(\tilde{\omega}_n^2)}{\vec{k}^2+\tilde{\omega}_n^2+M_0^2(\tilde{\omega}_n^2)}. \quad (11)$$

and we use the ultraviolet cut-off $\Lambda^2 = 1$ GeV^2. The confinement order parameter is defined through the function [8]

$$\Delta(\tau) = T \sum_n e^{i\omega_n \tau} \frac{M_0(\tilde{\omega}_n^2)}{\tilde{\omega}_n^2 + M_0^2(\tilde{\omega}_n^2)}. \tag{12}$$

According to the axiom of reflection positivity, if $\Delta(\tau)$ is positive for all τ, then the particle is stable, otherwise is confined. The inverse of the value of τ at which the first crossing occurs ($\tau > 0$) is taken as the order parameter for confinement.

4. Discussion and Conclusion

We solve the gap equation Eq.(2) for different Matsubara frequencies. We then calculate the chiral quark condensate at values of the temperature and fit with Lattice data [5] at finite temperature to determine the parameters of $\zeta(T)$ in eq. (10). The comparison of our fitted condensate versus the lattice data is shown in Fig. 1. Our gap equation solution provide us the full plateau for evolution of the chiral quark condensate from lower to higher temperature domain.

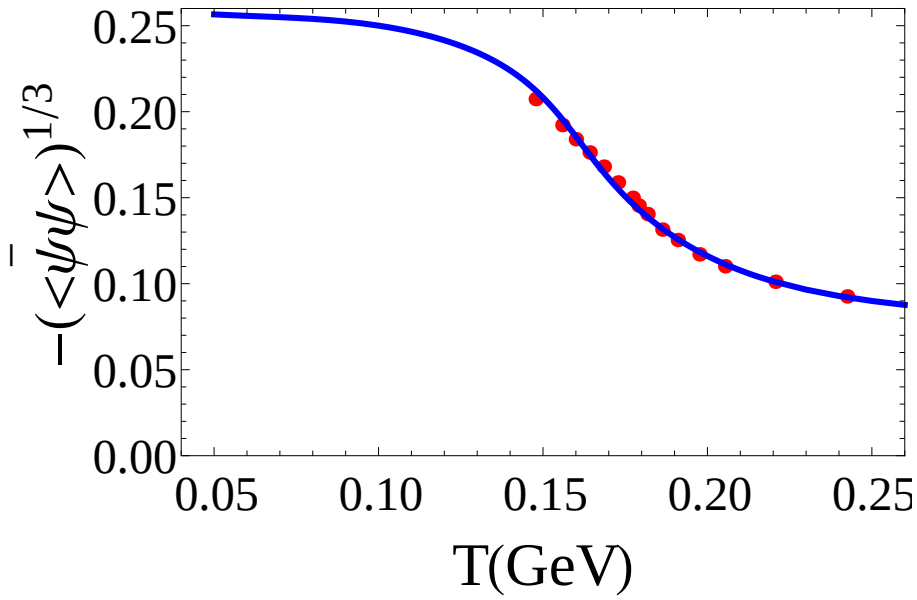

Figure 1. Chiral condensate as a function of temperature and at zero chemical potential: the blue curve represent the CMA result, while the red dots are the Lattice QCD data for the chiral condensate.

Working with finite quark masses, the chiral condensate is not a true order parameter for the chiral transitions. Nevertheless, we still can extract the pseudo-critical temperature by taking the derivative of the condensate, with respect to the temperature i.e., the temperature gradient of the chiral condensate as shown in Fig. 2. The maximum lies at $T_c = 0.161$ GeV (pseudo-critical temperature), while for Lattice it is $T_c^{lat} = 0.154$ GeV. According to the Lattice prediction, the mentioned pseudo-critical temperature at zero chemical potential is the origin of the cross over phase transition in the QCD phase diagram.

Next, we include the quark chemical potential μ_q (or baryonic chemical potential $\mu_B = 3\mu_q$) and calculate the chiral quark condensate. It is plotted as a function of the temperature for different values of the chemical potential in Fig. 3. The plot shows smooth pointwise

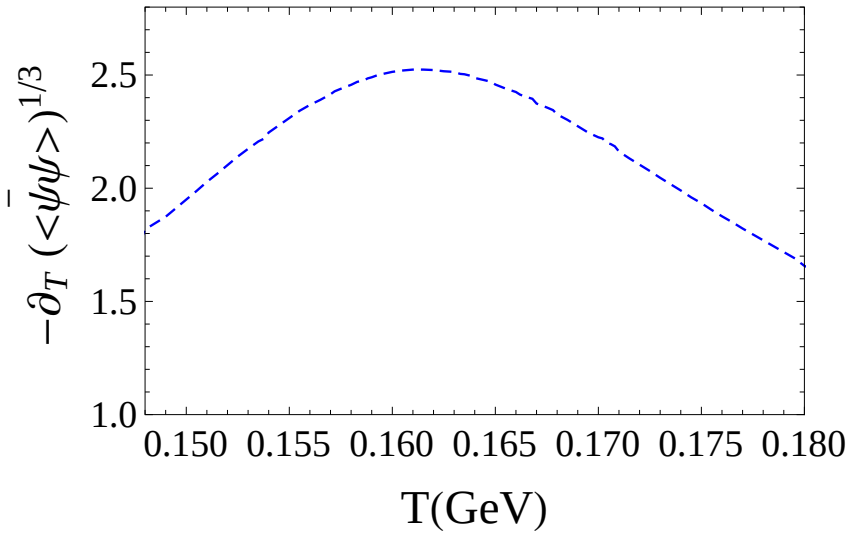

Figure 2. The thermal gradient of the chiral condensate, peak at $T = 0.161$ GeV and at zero chemical potential.

evolution of the condensate upto $\mu_q = 0.07$ ($\mu_B = 0.210$) GeV, while for higher than $\mu_q = 0.07$ ($\mu_B = 0.210$)GeV, a discontinuity occurs.

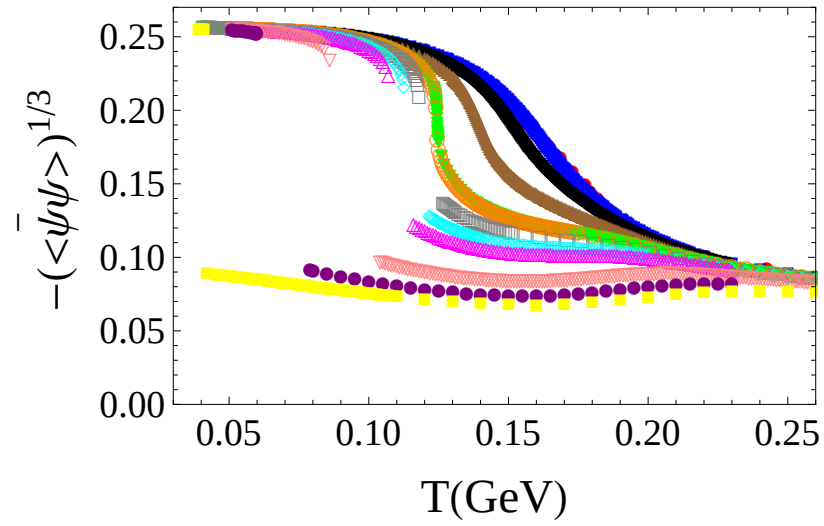

Figure 3. Chiral quark condensate as function of temperature and chemical potential: red dots represent Lattice QCD data at $\mu_q = 0$ GeV, CM Result: blue squares represent, $\mu_q = 0$ GeV , black diamonds,$\mu_q = 0.03$ GeV, brown triangles $\mu_q = 0.05$ GeV, Green inverted triangles $\mu_q = 0.07$ GeV, orange open circles $\mu_q = 0.0705$ GeV, gray open squares$\mu_q = 0.08$ GeV, cyan open diamonds, $\mu_q = 0.09$ GeV, pink open triangles $\mu_q = 0.1$ GeV, magenta inverted open triangles $\mu_q = 0.15$ GeV, purple circles $\mu_q = 0.2$ GeV, yellow squares $\mu_q = 0.25$ GeV.

In Fig. 4 we take the temperature gradient of the chiral quark condensate for different values of chemical potential. The plot shows the highest change occurs near $T_E = 0.1245$ GeV and

chemical potential $\mu_{q_E} = 0.07044$ ($\mu_{B_E} = 0.21132$) GeV.

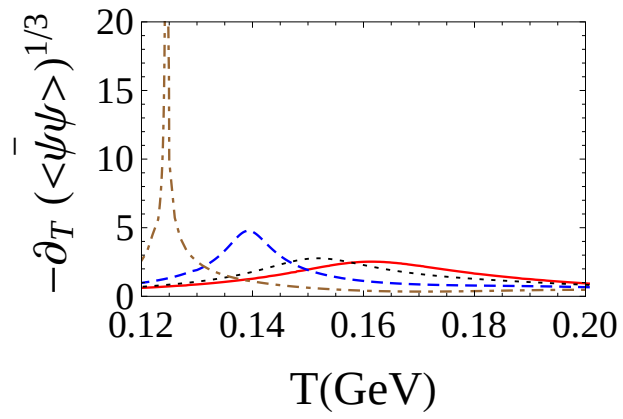

Figure 4. The thermal derivative of the chiral condensate at different chemical potential: red line represent $\mu_q = 0$ GeV, black dots represent $\mu_q = 0.03$ GeV, blue dashes represent $\mu_q = 0.05$ GeV, brown dashed dots $\mu_q = 0.07$ GeV.

In Fig. 5 we plot $\nu_T(\mu_B)$ i.e, the height of the thermal gradient $-\partial_T \langle\bar{\psi}\psi\rangle^{1/3}_{\mu_B}$ as a function of temperature for different value of the chemical potential. It shows the domains where different transitions occur. The $\nu_T(\mu_B)$ drawn on the vertical line, becomes singular as it approaches the dashed line, suggesting a change in the nature of phase transition from a simple cross-over to a first order phase transition.

We draw QCD phase diagram in Fig. 6, where temperature is along the vertical axis and baryonic potential μ_B along the horizontal axis. We locate the critical end point of the cross over and start of a first order phase transitions at ($T_E = 0.1245$ GeV, $\mu_E = 0.21132$ GeV). Thus we find that CMA approach describes that, there is cross-over in small region of chemical potential, while at higher chemical potential the transition becomes of first order. There are chiral symmetry breaking and restoration and confinement-deconfinement transition. Other approaches, which include chiral models and NJL-inspired models, place this point in the region $(\mu_E/T_c, T_E/T_c) \sim$ (1.0 - 2.0, 0.4 - 0.8) [9], whereas some mathematical extensions of lattice techniques [10] yield $(\mu_E/T_c, T_E/T_c) \sim$ (1.0 - 1.4, 0.9). We observe that the location $(\mu_E/T_c, T_E/T_c) \sim$ (1.3,0.7) established by the CMA gives a smaller value of μ_E than the one derived from a truncation of the gap equation considering the full momentum dependence of the quark propagator [6], but in fair agreement with other approaches. It could be due to the lack of control of the confinement scale with the chemical potential in the effective kernel of the gap equation. This issue and details of the confinement test will be addressed elsewhere [11].

Acknowledgments
We acknowledge CONACYT and IFM-UMSNH for support. AA acknowledges support to the organizers of the XIV MWPF, Oaxaca 2013. We also acknowledge Axel Weber for valuable discussions.

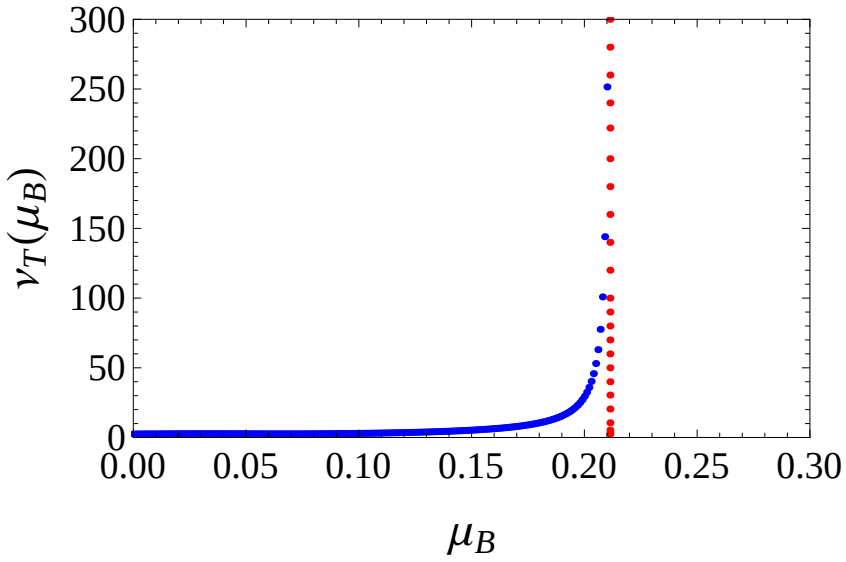

Figure 5. The height of the thermal derivative $\nu_T(\mu_B)$ is plotted as a function of the baryonic chemical potential (μ_B), that shows the domains where different transitions occur.

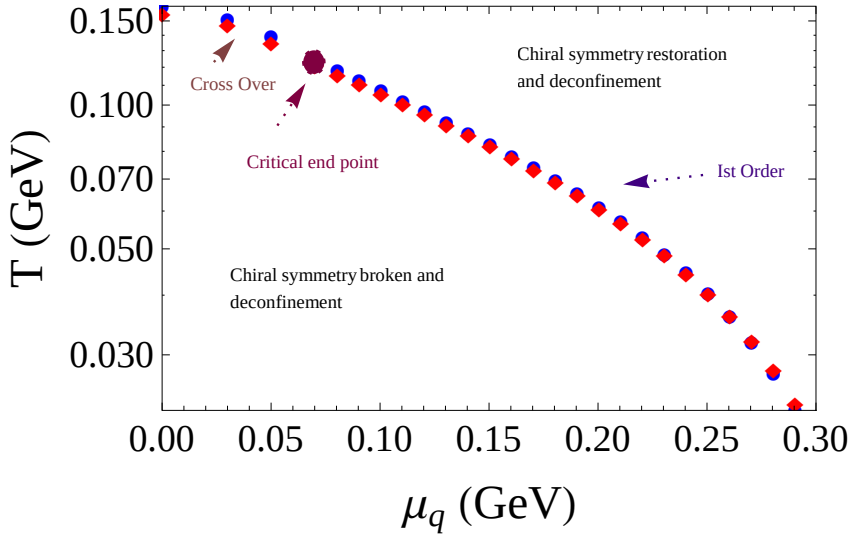

Figure 6. QCD phase diagram: Temperature vs baryonic chemical potential, the red diamonds represent the confinement-deconfinement transition, while the blue circles represent the chiral symmetry breaking-restoration. The purple dot represent the critical end point at ($T_E = 0.1245$ GeV, $\mu_E = 0.21132$ GeV).

References

[1] Aznauryan I G *et. al.* 2013, *Int. J. Mod. Phys. E* **22** 1330015.
[2] Bashir A, Raya A and Rodriguez-Quintero J 2013, *Phys. Rev. D* **88** 054003.
[3] Ahmad A and Raya A 2013, *Jour. Phys. Conf. Ser.* **418** 012009.
[4] Alkofer R, Fischer C S, Smekal L V 2002, *Phys. Rev. D* **52** 191;
Maris P, Raya A, Roberts C D and Schmidt S M, 2003,*Eur. Phys. J. A***18** 231 .
[5] Bazavov A, Bhattacharya T, Cheng M, DeTar C, Ding H T, Gottlieb S, Gupta R, Hegde P, Heller U M,

Karsch F 2012,*Phys. Rev. D* **85** 054503.
[6] Gutierrez E, Ahmad A, Ayala A, Bashir A, Raya A 2013, arXiv: 1304.8065v1 [hep-ph] .
[7] Klimenko K G 1992, *Z. Phys. C* **54** 323;
Gusynin V P, Miransky V A, Shovkovy I A 1995, *Phys. Rev. D* **52** 4747;
Gusynin V P, Miransky V A, Shovkovy I A 1996, Nucl. *Phys. B* **464** 249.
[8] Roberts C D 1998, arXiv: 9806088v1 [nucl-th];
Roberts C D (1999), *Phys. Part.Nucl* **30** 223.
[9] Schaefer B J, Pawlowski J M and Wambach J 2007, *Phys. Rev. D* **76** 074023;
Kovács P and Szép Z 2008, *Phys. Rev. D* **77** 065016;
Sasaki C, Friman B and Redlich K 2008, *Phys. Rev. D* **77**, 034024;
Costa P, Ruivo M C and de Sousa C A 2008, *Phys. Rev. D* **77** 096001;
Fu W-j, Zhang Z and Liu Y-x 2008, *Phys. Rev. D* **77** 014006;
Abuki H, Anglani R, Gatto R, Nardulli G and Ruggieri M 2008, *Phys. Rev. D* **78** 034034;
Schaefer B J and Wagner M 2009, *Phys. Rev. D* **79** 014018;
Costa P, Hansen H, Puivo M C and de Sousa C A 2010, *Phys. Rev. D* **81** 016007;
Loewe M, Marquez F and Villavicencio C 2013, *Phys. Rev. D* **88** 056004;
[10] Fodor Z and Katz S D 2002, *J. High Energy Phys.* **03** 014;
Gavai R V and Gupta S 2005, *Phys. Rev. D* **71** 114014 ;
de Forcrand P and Kratochvila S 2006, *Nucl. Phys. B, Proc. Suppl.* **153** 62;
Li A, Alexandru A, Meng X, and Liu K F 2009, *Nucl. Phys. A* **830** 633C.
[11] Ahmad A *et. al.* 2014, work is in progress .